論文 / 著書情報
Article / Book Information

Title	High pressure–temperature picosecond acoustic measurements on Fe using an internal-resistive-heated diamond anvil cell
Authors	Yoshihiro Nagaya, Takashi Yagi, Ryoto Ebina, Kei Hirose, Manabu Kodama, Shuichiro hirai, Kenji Ohta
Citation	HIGH PRESSURE RESEARCH, , ,
Pub. date	2025, 6
DOI	https://doi.org/10.1080/08957959.2025.2520559
Creative Commons	Information is in the article.

Taylor & Francis
Taylor & Francis Group

High Pressure Research
An International Journal

ISSN: 0895-7959 (Print) 1477-2299 (Online) Journal homepage: www.tandfonline.com/journals/ghpr20

High pressure–temperature picosecond acoustic measurements on Fe using an internal-resistive-heated diamond anvil cell

Yoshihiro Nagaya, Takashi Yagi, Ryoto Ebina, Kei Hirose, Manabu Kodama, Shuichiro Hirai & Kenji Ohta

To cite this article: Yoshihiro Nagaya, Takashi Yagi, Ryoto Ebina, Kei Hirose, Manabu Kodama, Shuichiro Hirai & Kenji Ohta (28 Jun 2025): High pressure–temperature picosecond acoustic measurements on Fe using an internal-resistive-heated diamond anvil cell, High Pressure Research, DOI: 10.1080/08957959.2025.2520559

To link to this article: https://doi.org/10.1080/08957959.2025.2520559

Published online: 28 Jun 2025.

HIGH PRESSURE RESEARCH
https://doi.org/10.1080/08957959.2025.2520559

Taylor & Francis
Taylor & Francis Group

High pressure–temperature picosecond acoustic measurements on Fe using an internal-resistive-heated diamond anvil cell

Yoshihiro Nagaya[a], Takashi Yagi [b], Ryoto Ebina[a], Kei Hirose[c], Manabu Kodama[d], Shuichiro Hirai[d] and Kenji Ohta[a]

[a]Department of Earth and Planetary Sciences, Tokyo Institute of Technology, Meguro, Japan; [b]National Metrology Institute of Japan, National Institute of Advanced Industrial Science and Technology, Ibaraki, Japan; [c]Department of Earth and Planetary Science, The University of Tokyo, Bunkyo, Japan; [d]Department of Mechanical Engineering, Tokyo Institute of Technology, Meguro, Japan

ABSTRACT

We determined the longitudinal wave velocity (V_P) of Fe up to 54 GPa and 2040 K by integrating picosecond acoustics with an internal-resistive-heated diamond anvil cell (DAC). Additionally, we performed *in-situ* measurements of sample thickness within the DAC using laboratory-based X-ray absorption imaging. The high pressure–temperature V_P values of Fe obtained in this study show strong agreement with those previously determined through synchrotron-based inelastic X-ray scattering experiments and ultrasonic measurements. The combination of picosecond acoustics, internal resistive heating, and X-ray absorption imaging provides a powerful approach for measuring the elastic wave velocities of Fe-based alloys under conditions relevant to terrestrial cores, thereby contributing to the understanding of their chemical composition.

ARTICLE HISTORY
Received 19 September 2024
Accepted 10 June 2025

KEYWORDS
Sound velocity; picosecond acoustics; high pressure; Fe

1. Introduction

Terrestrial bodies such as Earth, the Moon, Mars, and Mercury are believed to possess metallic cores primarily composed of Fe [1–4]. However, the precise structure and chemical composition of these cores remain a subject of debate. Understanding their composition and structure provides critical insights into planetary formation and evolution [3]. From a geophysical perspective, investigating the elastic properties of Fe alloys under high-pressure–temperature (P–T) conditions is essential for constraining core composition and crystal structure [5,6]. The density and sound velocity of the materials constituting planetary cores must be consistent with observational values under corresponding core P–T conditions. Birch's law, which describes a linear relationship between density and sound velocity, enables extrapolation from limited experimental data in relatively low-

CONTACT Yoshihiro Nagaya nagaya.y.c1cb@m.isct.ac.jp

pressure range, facilitating comparisons with one-dimensional density and seismic wave velocity profiles along planetary radii.

Advancements in planetary exploration are expected to provide more detailed velocity profiles of the cores of terrestrial bodies. Recent observations from NASA's *InSight* mission suggest that Mars either lacks a solid inner core or possesses only a small one [2]. Additionally, the BepiColombo mission, launched in 2017, is expected to elucidate Mercury's internal structure through a series of scientific experiments scheduled for 2025 [7]. As seismological data on terrestrial planets continue to expand, developing efficient methods to obtain sound velocity data at high *P*–*T* conditions in laboratory settings is crucial for providing geophysical insights into planetary interiors.

Picosecond acoustics has recently gained attention as a promising technique for measuring the sound velocity of metal samples under high-pressure conditions. In this method, a femtosecond pulsed laser generates high-frequency (∼10 GHz) elastic waves. This high frequency is essential because high-pressure samples in diamond anvil cells (DACs) are typically thinner than 10 μm, making lower-frequency (MHz) waves – with longer wavelengths – unsuitable for propagation. Therefore, this technique is well-suited for sound wave velocity measurements in thin, high-pressure samples. Additionally, this technique enables rapid laboratory-based measurements, typically requiring less than one hour per experiment, which is considerably shorter than methods conducted at synchrotron radiation facilities. Previous studies have successfully applied this technique to investigate the elastic properties of Fe and Fe alloys containing nickel or hydrogen at pressures exceeding 100 GPa [8–10].

In this study, we introduced two novel approaches to measure the elastic wave velocities of Fe at high *P*–*T* conditions. The first involves an internal resistive heating technique, which enables stable high-temperature conditions. Using this approach, we determined the compressional wave velocity (V_P) of Fe up to 54 GPa and 2040 K. The second involves laboratory-based X-ray absorption imaging, which allowed *in-situ* measurements of sample thickness during compression up to 50 GPa and room temperature. Our experimental *P*–*T* range encompasses almost the entire core conditions of Mars, Mercury, Venus, and the Moon, providing valuable insights into the elastic properties of planetary cores.

2. Methods

We conducted a series of picosecond acoustics (PA) measurements using an optical system installed at Institute of Science Tokyo (Figure 1) [11,12]. A high-power femtosecond pulsed laser (Fidelity-2, Coherent Corporation, USA) with a wavelength of 1070 nm, a pulse width of 55 fs, and a repetition rate of 70 MHz was employed. The laser beam was split into pump and probe beams using a polarizing beam splitter. The pump beam was modulated into a 1 MHz square wave by an acousto-optic modulator (AOM) and irradiated onto one side of the sample with a spot diameter of <10 μm and a power of approximately 30 mW to generate sound waves. The probe beam passed through a lithium triborate crystal, where it was frequency-doubled to generate its second harmonic at 535 nm. This wavelength conversion was implemented to enable selective filtering of the pump beam, which has a higher intensity than the probe beam, in order to prevent potential damage to the detector caused by pump light

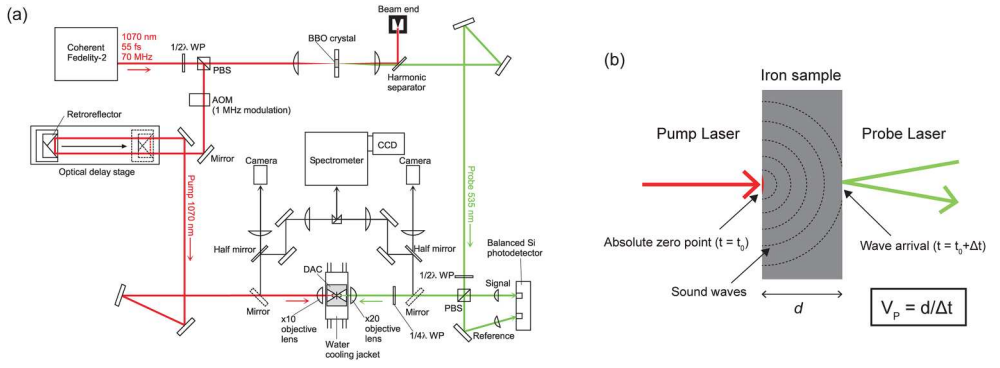

Figure 1. (a) The schematics of the optical line for picosecond acoustics. Lines colored red and green indicate the pump laser (1070 nm) and the probe laser (535 nm), respectively. The black line indicates the ray path of thermal radiation from the sample. (b) Schematics of the picosecond acoustics measurement. The pump laser generates a coherent acoustic wave at the optical zero point ($t = t_0$). The optical delay stage adjusts the optical path length of the pump laser, effectively controlling the timing of pump-laser irradiation. When the pump laser irradiates the sample earlier than the probe laser by a time Δt, corresponding to the acoustic wave propagation time, the arrival of acoustic wave at a probe position is detected as an abrupt change in the intensity and/or phase of the reflected probe signal.

transmitted through the sample. Probe beam was then directed to the opposite side of the sample, with its power adjusted to approximately 5 mW. To enhance measurement accuracy, we detected the intensity and phase of the reflected probe beam using a balanced detector (2107-FS-M, Newport Corporation, USA), which improves the signal-to-noise ratio by subtracting temporal fluctuations in the reference light intensity from the raw signal [9]. For subsequent analysis, the signal component – either intensity or phase – with the higher signal-to-noise ratio was selectively used to ensure reliable identification of the wave arrival time (Figure 1 and Figure 2). Additionally, a lock-in amplifier (LI5660, NF corporation, Japan), tuned to the 1 MHz modulation frequency imposed by the AOM, was utilized to further improve the signal-to-noise ratio.

For high-pressure and high-temperature (P–T) generation, we utilized symmetric-type diamond anvil cells (DACs) in combination with an internal resistive heating technique [11]. Diamond anvils with a 300 μm flat culet were employed to generate high pressures. To ensure precise heating control, the Fe foil sample with 5N-purity was fabricated using an ultraviolet laser processing machine prior to loading into the sample chamber (Figure 3(b)). The surface of the pre-indented rhenium gasket was electrically insulated using a mixture of cubic boron nitride and titanium dioxide powder, along with cement (Resbond™ 919, Cotronics Corporation, USA). Platinum foils were placed on the insulating layer and connected to the metal sample and external copper wires, which served as electrodes. A stable high temperature was generated via Joule heating by applying a voltage to the conductor, inducing an electric current flow [11,13] (Figures 4 and 5).

Pressure was measured at room temperature using the ruby fluorescence technique. The uncertainty in pressure was calculated following the methodology outlined in a previous study [14]. The temperature conditions during the experiments were determined based on the wavelength profile of the radiant light, measured using a spectrometer

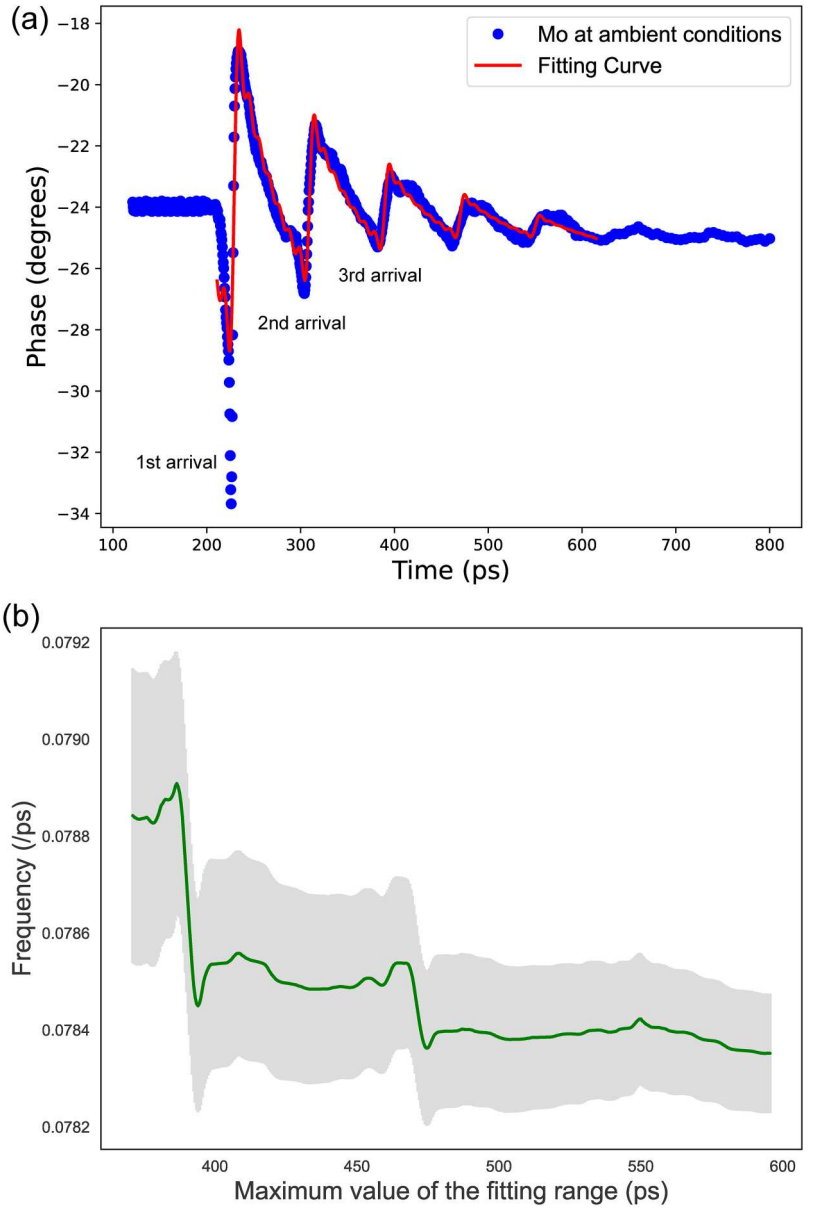

Figure 2. (a) Temporal evolution of the phase value of the probe laser (blue plot) and the fitted curve using a sawtooth wave function (red line) are shown. From this analysis, we determined the frequency of wave arrivals propagating back and forth across the film. (b) Extracted frequency values as function of different fitting ranges, demonstrating that the result is largely independent of the fitting window. The obtained frequency is 0.0787(5) ps^{-1}, corresponding to a round-trip time of 79.8(5) ps for an elastic wave traversing the sample.

(SP-2156-DAC Teledyne Princeton Instruments, USA) and a CCD camera (PIXIS256E-DAC Teledyne Princeton Instruments, USA). Wavelength calibration of the CCD camera was performed using a neon lamp. To account for the absorption of radiant light by optical components, we measured the radiation spectrum of a calibrated tungsten lamp.

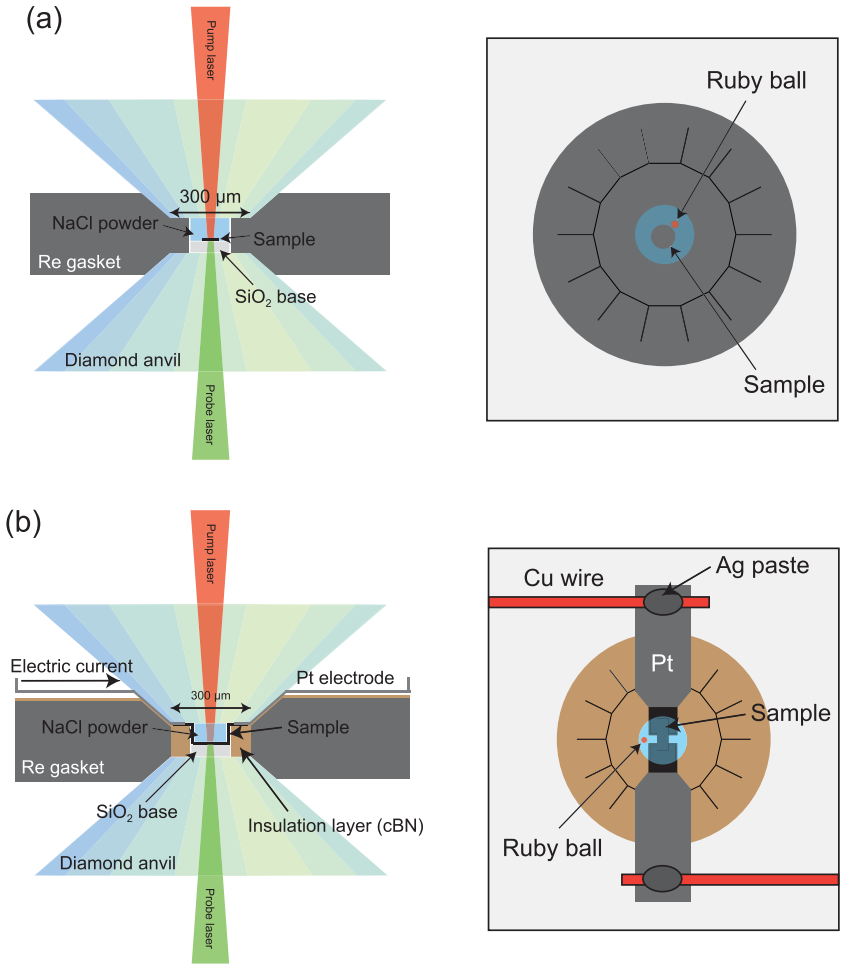

Figure 3. (a) Sample configuration for picosecond acoustic measurements under high-pressure and room-temperature conditions. (b) Sample configuration of the internal-resistive-heated diamond anvil cell. In both experimental setups, a metal sample was placed on a SiO_2 substrate to enhance optical reflectivity and covered with NaCl, which served as both a pressure medium and a thermal insulator. A ruby sphere was positioned near the sample within the sample chamber for pressure determination.

By comparing the measured spectrum with the ideal blackbody profile, we estimated the spectral absorption effect introduced by the optical components and applied this correction in the temperature determination [15]. The temperature prior to each picosecond acoustics measurement was determined by two-color analysis to the radiant light profile (Figure 5) [16].

To determine the pressure during high-temperature measurements, we evaluated the thermal pressure of the sample. Previous studies have described thermal pressure during heating in high pressure apparatus to be 2.4 MPa/K, 60% of the theoretical thermal pressure $\alpha K_T \Delta T$, where α is the thermal expansion coefficient and K_T is the isothermal bulk modulus [15,17]. We adopted the 10% pressure error during high-T experiments. The remaining 40% of the theoretical thermal pressure causes thermal expansion of

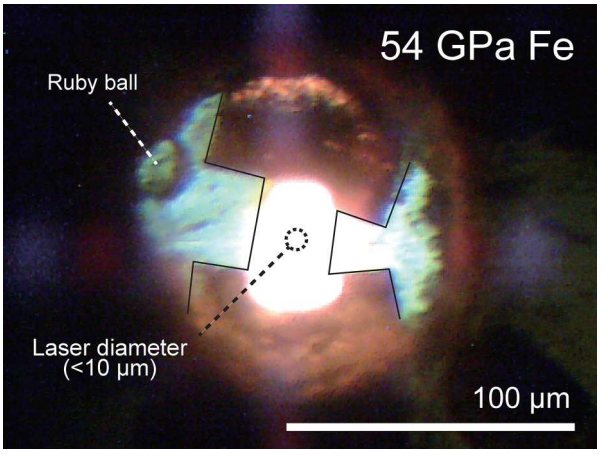

Figure 4. A photograph of the sample chamber in an internal-resistive-heated DAC at 54 GPa. The Fe sample was heated by applying direct current. The diameter of the pump and probe lasers for picosecond acoustics is shown as the circle.

the sample, thereby influencing its thickness d. At room temperature, the longitudinal wave velocity (V_P) is determined based on the travel time (t) and sample thickness (d) using the following equation:

$$V_P = \frac{d}{t} \tag{1}$$

Under high-temperature conditions, the relationship between the sound velocity at high temperature (V_P^{HT}) and at room temperature (V_P^{RT}) can be expressed as:

$$V_P^{HT} = \frac{\alpha}{t^{HT}/t^{RT}} V_P^{RT} \tag{2}$$

where α represents the expansion rate in thickness. Here, t^{HT} and t^{RT} denote the travel time of sound at high and room temperatures, respectively, both of which are directly obtained from picosecond acoustics measurements. The V_P^{HT} value was determined under the assumption of isotropic thermal expansion, where α is given by:

$$\alpha = \left(\frac{v^{HT}}{v^{RT}}\right)^{1/3} \tag{3}$$

The error range was estimated by considering two limiting cases: no thermal expansion ($\alpha = 0$) and uniaxial thermal expansion ($\alpha = v^{HT}/v^{RT}$). The unit cell volumes at high temperature (v^{HT}) and ambient temperature (v^{RT}) were determined using thermal equations of states [12,18,19]. The room-temperature compressional wave velocity (V_P^{RT}) was adopted from Sakamaki et al. [20]. After high P–T picosecond acoustic measurements, we collected the synchrotron X-ray diffraction (XRD) patterns of samples without decompression at ambient temperature, at BL10XU, SPring-8, Japan [21]. This was performed as a basic check to ensure that no unexpected chemical reactions, such as carbon contamination from the diamond anvils, had occurred during high-temperature experiments.

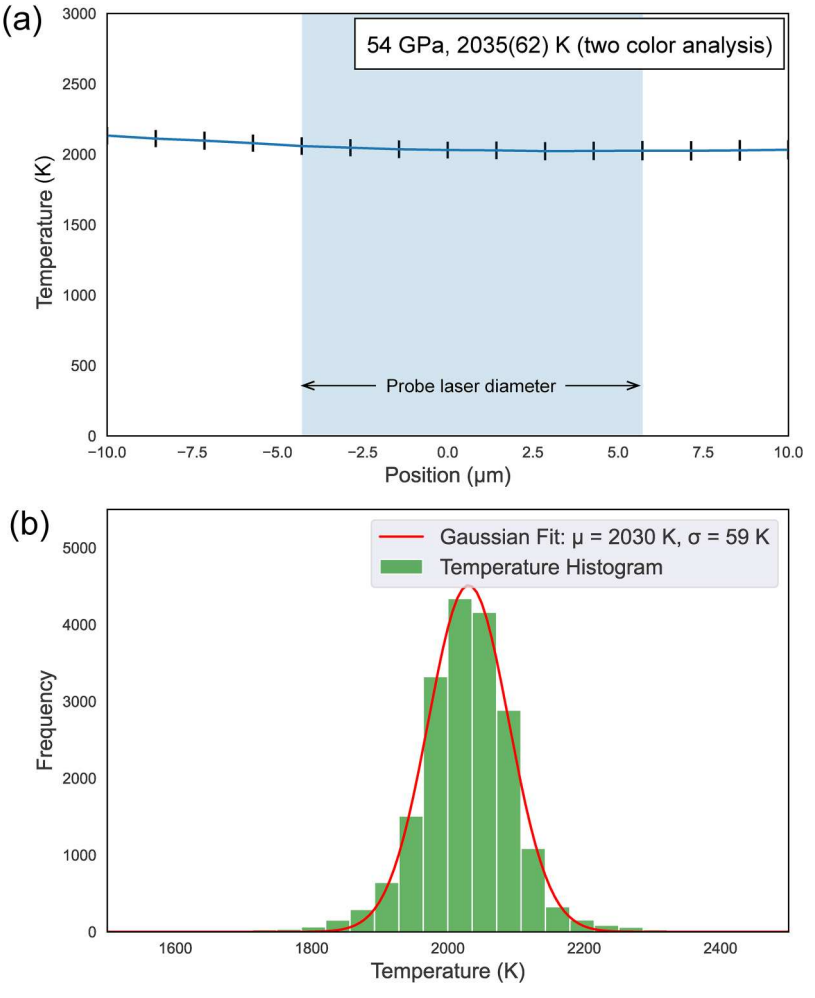

Figure 5. (a) Temperature profile along the sample surface, calculated using two-color analysis. The horizontal axis represents the sample position, with the zero-position defined as the point where the intensity of the radiant light is strongest. The blue-shaded region indicates the probe laser diameter for picosecond acoustics measurements. The temperature was determined by averaging over a ± 5 μm area, yielding a spatial temperature uncertainty of 62 K at 2035 K (3.05%) in this measurement. Considering temporal temperature variations, the overall experimental temperature uncertainty was estimated to be 5%. (b) Result of the two-color analysis. The temperature histogram was fitted with a Gaussian distribution.

We determined the travel time of sound waves based on the absolute zero point and the wave arrival point. The absolute zero point corresponds to the moment when the sound waves begin propagating at the sample surface. To establish this reference, we measured the PA signal of a 400 nm-thick Mo thin film sputtered onto a glass substrate. In the PA signal, we observed oscillations corresponding to repetitive wave arrivals propagating back and forth within the Mo film. To quantify the wave arrival frequency, we applied a fitting procedure using a sawtooth function, as described below.

$$f(t, A, \omega, \alpha, \beta, \varphi, \gamma) = \sum_{n=1}^{7} A\left(\frac{1}{n}\sin(n\omega(t+\beta))\exp(-\alpha t) + \varphi t + \gamma\right) \quad (4)$$

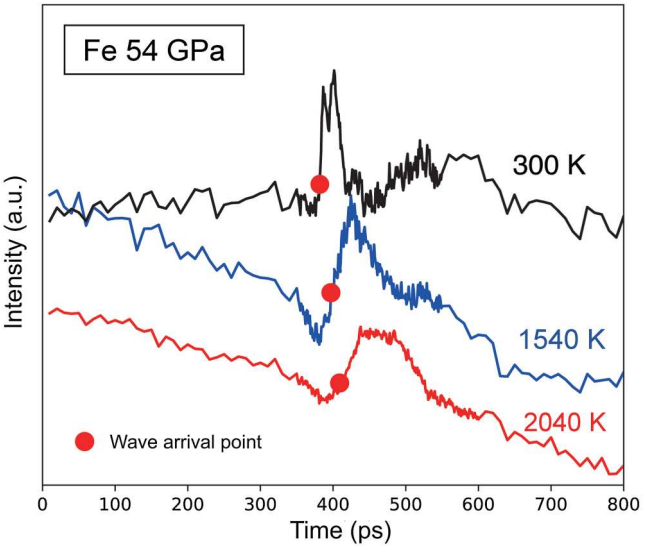

Figure 6. The obtained picosecond acoustic signals of Fe obtained at 54 GPa vary with increasing temperature. Red points indicate the times when the elastic wave first arrived at the sample surface of the probe laser side.

The fitting analysis yielded an angular frequency ω of 0.0787(5) ps^{-1} (see Figure 6 for details). This frequency corresponds to a wave arrival interval of 79.8(5) ps, indicating that the absolute zero point precedes the first wave arrival by 39.9(5) ps.

It is essential to account for the influence of transparent materials, such as the glass substrate and diamond anvils, as their higher refractive indices compared to air change the focal position of the objective lens. Since the position of the probe-side lens remained fixed throughout our experiments, we quantified the deviation of the absolute zero point. The focal length shift Δf induced by a material with thickness d and refractive index n is given by $\Delta f = d(1 - 1/n)$. Within the pressure range of our measurements, the refractive index of diamond is 2.45(5). For a diamond anvil with 2.0(2) mm, the focal shift is calculated as 1.2(1) mm, corresponding to a time shift of 3.9(4) ps. To account for this effect, we applied a correction of −7.8 ps to the absolute zero point, incorporating the influence of the pump-side anvil. Additionally, the effect of the glass substrate must also be considered. The glass substrate, with a thickness of 0.5 mm and a refractive index of approximately 1.5(1), introduces an additional focal shift of 0.17(1) mm. Consequently, we applied a final correction of −7.4 ps to the absolute zero point, ensuring that the influence of both the diamond anvils and the glass substrate was appropriately addressed. The uncertainty associated with this correction has been incorporated into the overall travel time error estimation.

In the high-pressure and room-temperature travel time measurements, the *in-situ* sample thickness within the DAC was determined using the X-ray absorption method. While previous picosecond acoustics studies have typically estimated sample thickness under high-pressure conditions by extrapolating from its ambient value using the equation of states of the sample [8–10,22,23], direct measurement of the *in-situ* sample thickness is preferable for improving the accuracy of sound velocity determinations.

Figure 3(a) presents a schematic of the sample configuration. A metal sample with an initial thickness of approximately 10 μm was loaded into a sample chamber within a pre-indented Re gasket. A polycrystalline SiO_2 base and NaCl powder were used as the pressure medium. To accurately measure the sample thickness, we utilized a laboratory-based X-ray microscope (Rigaku nano3DX) [24], which employs characteristic Kα X-rays of Mo (λ = 0.70926 Å). The incident X-ray was directed parallel to the compression axis of the miniature DAC, and a projection image of the entire sample chamber was captured using a CMOS detector.

The sample thickness was determined by applying Lambert-Beer's law, using the intensities of the incident X-ray (I_0), the X-ray transmitted through the sample (I_1), and the X-ray transmitted through a region of the sample chamber without the sample (I_2). The following relationships were obtained:

$$\ln\left(\frac{I_1}{I_0}\right) = -(\mu_s \rho_s l + \xi) \tag{5}$$

$$\ln\left(\frac{I_2}{I_0}\right) = -(\mu_{pm} \rho_{pm} l + \xi), \tag{6}$$

where μ_s and μ_{pm} are the X-ray absorption coefficients per unit density and unit length of the metal sample and the pressure medium, respectively, ρ_s and ρ_{pm} are the densities of the sample and the pressure medium, l is the thickness of the sample, and ξ accounts for X-ray absorption by components other than the sample, such as the diamond anvils or SiO_2 plate. The values of I_1 and I_2 were obtained by averaging the X-ray counts within a circular region of 5 μm in diameter, corresponding to the probe laser spot size. By eliminating I0 from equations (2) and (3), the following expression is derived:

$$\ln\left(\frac{I_1}{I_2}\right) = -(\mu_s \rho_s - \mu_{pm} \rho_{pm}) l. \tag{7}$$

For the calculations, we adopted X-ray absorption coefficients per unit density and unit length of 36.38 cm^2/g for the Fe sample and 7.55 cm^2/g for the NaCl pressure medium [25]. The densities of Fe and NaCl were determined using their respective equations of state [18,26].

3. Results & discussion

3.1. Temperature dependence of the sound velocity of Fe

We conducted high-*P*–*T* picosecond acoustics measurements on Fe over a total of four experimental runs, comprising hexagonal close-packed (hcp) Fe (two runs), face-centered cubic (fcc) Fe (one run), and body-centered cubic (bcc) Fe (one run). XRD measurements were performed to identify the sample phase after the high-temperature picosecond acoustics measurements. In all experiments, no XRD patterns from Fe-light element alloys, such as Fe-carbide, were observed. Table 1 summarizes the data for pure Fe up to 54 GPa and 2040 K. The temperature distribution remained nearly uniform within the spatial range corresponding to the picosecond acoustics laser diameter (<10 μm) (Figure 5(a)). The temperature uncertainty was calculated by taking into account the error propagation of individual temperature values at each point in the profile data, which represents the temperature

Table 1. Experimental data at high temperature

Run name	Phase	P (GPa)	T (K)	ρ (g/cm^3)	a (isotropic)	a (uniaxial)	t.t. (ps)	V_P (km/s)	lower error	upper error
1	hcp + fcc	54(5)	1540(77)	7.59(15)	1.0067	1.0202	237(3)	7.69	0.05	0.10
		54(5)	1620(81)	7.43(15)	1.0072	1.0219	242(3)	7.53	0.05	0.11
		55(5)	2040(102)	7.20(14)	1.0097	1.0294	249(3)	7.34	0.07	0.14
2	hcp	52(5)	1600(80)	7.40(15)	1.0072	1.0217	275(3)	7.50	0.05	0.11
3	fcc + hcp	20(2)	1140(57)	8.64(17)	1.0068	1.0205	456(3)	6.48	0.04	0.09
		21(2)	1230(62)	8.62(17)	1.0074	1.0224	446(3)	6.62	0.05	0.10
		21(2)	1400(70)	8.59(17)	1.0093	1.0283	459(3)	6.45	0.06	0.12
4	bcc	6.6(7)	1100(55)	7.99(16)	1.0085	1.0256	565(3)	5.88	0.05	0.10

distribution, yielding an error of 3% (Figure 5(b)). Considering the temporal variation during the picosecond acoustic measurements, the overall experimental temperature uncertainty was estimated to be 5%. This uncertainty is approximately half that of conventional laser heating experiments, which typically exhibit temperature uncertainties of 10% [22].

We acquired the picosecond acoustic signals at several temperatures up to 2040 K (Figure 2). At all temperature conditions, intensity measurements were performed with high temporal resolution (1 ps) around the acoustic signal to minimize the overall measurement duration. In certain runs, a slight drop in intensity was observed immediately prior to a pronounced increase. This dip is attributed to the interference between light penetrating a finite depth at the sample surface and light scattered by the acoustic pulse at that depth [27]. Consequently, we interpreted the abrupt intensity rise as the wave arrival and determined the wave arrival time using standard seismological methods, consistent with the previous studies [9,10].

As temperature increases, the arrival time of the elastic wave is delayed, and the acoustic signals become broader. These characteristics can be explained by two primary factors. The first is that a temperature dependence of the acoustic dispersion. Acoustic dispersion refers to the variation in phase velocity as a function of frequency for the propagating wave. If the frequency dependence of the phase velocity increases at high temperatures, the acoustic signal broadens correspondingly. The second factor is the temperature dependence of the electronic specific heat [27]. A localized temperature rise within a small region, known as the optical skin depth, generates sound waves from the edges of the sample. The sharpness of the acoustic signal is influenced by the rate of this temperature increase: a more rapid temperature rise results in a sharper acoustic signal. The timescale of this temperature increase is proportional to the square root of the electronic specific heat of the sample. Under high-temperature conditions, the timescale becomes longer, leading to a broader picosecond acoustic signal.

In all experimental runs, the sound velocity of Fe decreased at high temperatures compared to room-temperature conditions. Notably, at around 50 GPa, our sound velocity data exhibit good agreement with the velocity model based on previous inelastic X-ray scattering (IXS) studies conducted using the laser heating method (Figure 7) [20,28]. The sound velocity data at lower pressures also show good consistency with previous studies. At 4.6 GPa, XRD patterns of bcc Fe were observed after the picosecond acoustics measurements. Therefore, we determined the high-temperature V_P value at these pressures based on previous ultrasonic measurements for bcc Fe. The degree of temperature dependence obtained in this study was found to be consistent with values reported in the literature [29,30].

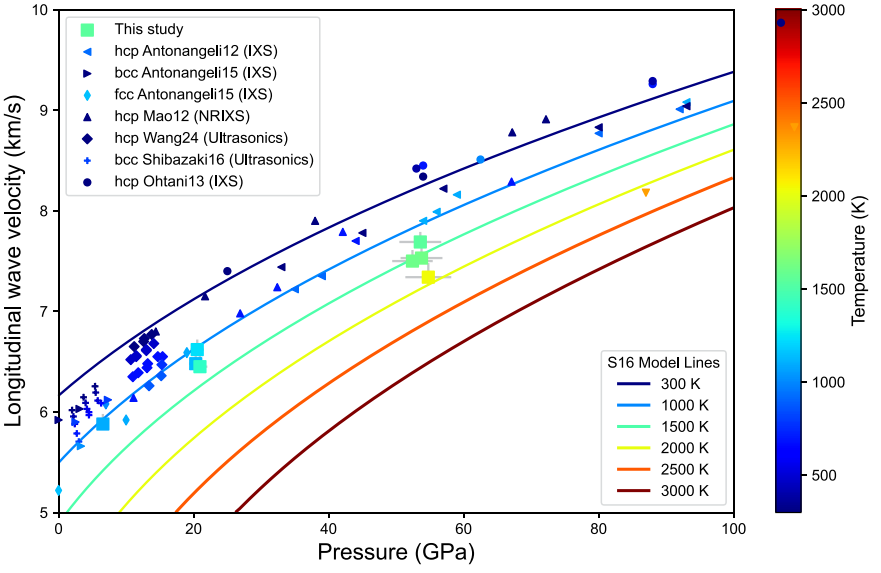

Figure 7. Pressure and temperature dependence of the longitudinal wave velocity (V_P) of Fe. Square markers represent the data obtained in this study. Other markers indicate results from previous studies, including inelastic X-ray scattering (IXS) measurements (left triangle: Antonangeli et al. [31]; circle: Ohtani et al. [32]; right triangle: bcc from Antonangeli et al. [29]; small diamond: fcc Fe from Antonangeli et al. [29]; downward triangle: Sakamaki et al. [20], nuclear resonant inelastic X-ray scattering (NRIXS) measurements (upward triangle: Mao et al. [33]), and ultrasonic measurements (+: Shibazaki et al. [30]; diamond: Wang et al. [34]). The solid lines represent the pressure-velocity relationship model for solid Fe as reported by Sakamaki et al. [20].

Additionally, our data around 20 GPa align well with the IXS data for fcc Fe from Antonangeli et al. [29]. These results indicate that our picosecond acoustics measurements successfully captured the sound velocities of Fe in these crystal structures at lower pressure conditions.

3.2. Sound velocity measurements with direct determination of the sample thickness

We applied 3×3 pixel^2 median filtering to the acquired X-ray transmission images to eliminate value overflow in the acquired transmission images (Figure 8). This overflow is mainly caused by the thermal noise, and noise due to cosmic rays. The resolution of the transmitted image is about 900 nm, corresponding to a filtering window size of ~2.7 μm. This value is smaller than the picosecond acoustic laser diameter (<10 μm).

We summarized the measured pressure, thickness, travel time, and compressional wave velocity of the compressed Fe films in Table 2. With increasing pressure, the sample thickness got thinner and the travel time got shorter and the V_P values got higher, consistent with the previous EOS and sound velocity measurements [8,18,35]. We calculated the thickness error to be between 2% and 3.5%. The absolute values of V_P are also consistent with results from previous studies using the picosecond acoustics method [8], IXS [28,29,31], NRIXS [33], and ultrasonic measurements [30,34] (Figure 9).

Table 2. Experimental data at ambient temperature.

Run#	P (GPa)	t.t. (ps)	d (μm)	V_P (km/s)
5	22.4(2)	1050(2)	7.54(15)	7.18(14)
	26.7(2)	900(2)	6.73(17)	7.48(19)
	39.5(4)	787(2)	6.27(22)	7.97(28)
	50.1(4)	724(2)	5.95(12)	8.22(17)

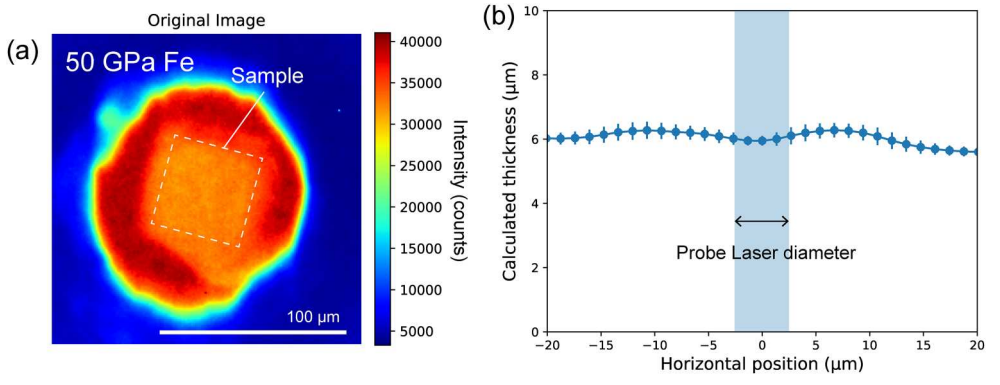

Figure 8. (a) X-ray absorption image of the sample chamber at 50.1 GPa and 300 K, and (b) thickness profile of the Fe sample. The color of each pixel represents the transmitted X-ray intensity. The rectangular region outlined by the dotted line denotes the Fe sample. The sample thickness was determined by averaging the calculated thickness within the region corresponding to the probe laser spot.

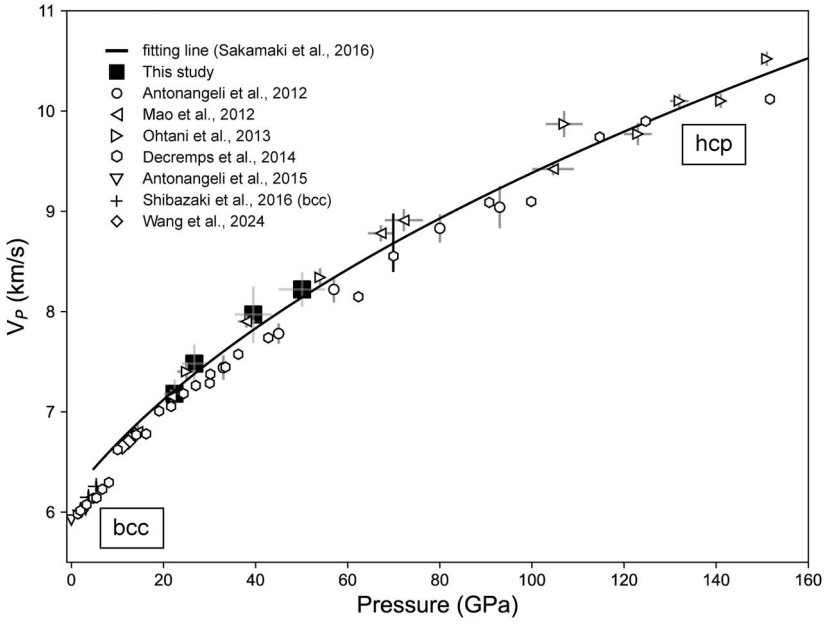

Figure 9. The pressure dependence of V_P at room temperature. Several markers indicate different literature (square: this study, circle: Antonangeli et al. [31], left triangle: Mao et al. [33], right triangle: Ohtani et al. [32], hexagon: Decremps et al. [36], downward triangle: Antonangeli et al. [29], plus: Shibazaki et al. [30], diamond: Wang et al. [34]). The solid black line is the sound velocity model from Sakamaki et al. [20] with the uncertainty shown as error bar.

4. Conclusion

This study measured elastic wave velocities of pure Fe up to 54 GPa and 2040 K loaded in an internal-resistive-heated diamond anvil cell. We also reported *in-situ* thickness measurements of compressed Fe film using a laboratory-based X-ray microprobe and produced the sound velocity at high pressure and room temperature. Our results agreed with those of previous studies using multiple techniques and supported the validity of our measurement scheme. The measured temperature and pressure regimes in this study are comparable to those of the cores of terrestrial planets such as Mars, Mercury, and Venus. This method can quickly collect the necessary elastic wave velocity data, giving significant insight into these core compositions.

Acknowledgements

We acknowledge Dr. Motonobu Tomoda, Dr. Yuji Higo, Dr. Junichi Nakajima, Dr. Hitoshi Gomi and Dr. Kotaro Hikosaka for helpful discussion. The synchrotron XRD measurements were conducted at BL10XU, SPring-8 (proposal no. 2023A0181 and 2023B1280). This work was supported by JSPS KAKENHI Grant Number 19H00716, 24KJ1090, and 21H04968. One of authors would like to acknowledge the support from the Hiki Foundation, Tokyo Institute of Technology. We used the ChatGPT −4o model to refine our manuscript and enhance the clarity of our English descriptions.

Author contribution

K.O. and Y.N. designed the study and wrote the manuscript. Y.N. carried out the experiments and was helped by K.O., T.Y., and M.K. R.E. supported data analysis. All authors discussed the results and commented on the manuscript.

Disclosure statement

No potential conflict of interest was reported by the author(s).

Funding

This work was supported by Japan Society for the Promotion of Science: [Grant Number 19H00716, 24KJ1090, 21H04968]; Hiki foundation.

Data availability statement

The datasets used and/or analyzed during the current study are available from the corresponding author on reasonable request.

ORCID

Takashi Yagi http://orcid.org/0000-0002-2008-872X

References

[1] Margot J-L, Hauck II SA, Mazarico E, et al. Mercury's internal structure. 2018 [cited 2025 Feb 2]. p. 85–113. Available from: http://arxiv.org/abs/1806.02024.

[2] Irving JCE, Lekić V, Durán C, et al. First observations of core-transiting seismic phases on Mars. Proc Natl Acad Sci USA. 2023;120(18):e2217090120. doi:10.1073/pnas.2217090120

[3] Hirose K, Wood B, Vočadlo L. Light elements in the Earth's core. Nat Rev Earth Environ. 2021;2(9):645–658. doi:10.1038/s43017-021-00203-6

[4] Weber RC, Lin P-Y, Garnero EJ, et al. Seismic detection of the lunar core. Science. 2011;331(6015):309–312. doi:10.1126/science.1199375

[5] Fiquet G, Badro J, Guyot F, et al. Sound velocities in iron to 110 gigapascals. Science. 2001;291(5503):468–471. doi:10.1126/science.291.5503.468

[6] Badro J, Fiquet G, Guyot F, et al. Effect of light elements on the sound velocities in solid iron: implications for the composition of Earth's core. Earth Planet Sci Lett. 2007;254(1):233–238. doi:10.1016/j.epsl.2006.11.025

[7] Benkhoff J, van Casteren J, Hayakawa H, et al. Bepicolombo – comprehensive exploration of mercury: mission overview and science goals. Planet Space Sci. 2010;58(1):2–20. doi:10.1016/j.pss.2009.09.020

[8] Decremps F, Antonangeli D, Gauthier M, et al. Sound velocity of iron up to 152 GPa by picosecond acoustics in diamond anvil cell. Geophys Res Lett. 2014;41(5):1459–1464. doi:10.1002/2013GL058859

[9] Wakamatsu T, Ohta K, Yagi T, et al. Measurements of sound velocity in iron–nickel alloys by femtosecond laser pulses in a diamond anvil cell. Phys Chem Minerals. 2018;45(6):589–595. doi:10.1007/s00269-018-0944-3

[10] Wakamatsu T, Ohta K, Tagawa S, et al. Compressional wave velocity for iron hydrides to 100 gigapascals via picosecond acoustics. Phys Chem Minerals. 2022;49(5):17. doi:10.1007/s00269-022-01192-8

[11] Zha C-S, Bassett WA. Internal resistive heating in diamond anvil cell for in situ x-ray diffraction and Raman scattering. Rev Sci Instrum. 2003;74(3):1255–1262. doi:10.1063/1.1539895

[12] Campbell AJ, Danielson L, Righter K, et al. High pressure effects on the iron–iron oxide and nickel–nickel oxide oxygen fugacity buffers. Earth Planet Sci Lett. 2009;286(3):556–564. doi:10.1016/j.epsl.2009.07.022

[13] Park Y, Yonemitsu K, Hirose K, et al. Viscosity of Earth's inner core constrained by Fe–Ni interdiffusion in Fe–Si alloy in an internal-resistive-heated diamond anvil cell. Am Mineral. 2023;108(6):1064–1071. doi:10.2138/am-2022-8541

[14] Shen G, Wang Y, Dewaele A, et al. Toward an international practical pressure scale: a proposal for an IPPS ruby gauge (IPPS-Ruby2020). High Press Res. 2020;40(3):299–314. doi:10.1080/08957959.2020.1791107

[15] Tateno S, Kuwayama Y, Hirose K, et al. The structure of Fe–Si alloy in Earth's inner core. Earth Planet Sci Lett. 2015;418:11–19. doi:10.1016/j.epsl.2015.02.008

[16] Kimura T, Murakami M. Fluid-like elastic response of superionic NH3 in Uranus and Neptune. Proc Natl Acad Sci USA. 2021;118(14):e2021810118. doi:10.1073/pnas.2021810118

[17] Mori Y, Ozawa H, Hirose K, et al. Melting experiments on Fe–Fe3S system to 254 GPa. Earth Planet Sci Lett. 2017;464:135–141. doi:10.1016/j.epsl.2017.02.021

[18] Dewaele A, Loubeyre P, Occelli F, et al. Quasihydrostatic equation of state of iron above 2 mbar. Phys Rev Lett. 2006;97(21):215504. doi:10.1103/PhysRevLett.97.215504

[19] Dorogokupets PI, Dymshits AM, Litasov KD, et al. Thermodynamics and Equations of State of Iron to 350 GPa and 6000 K. Sci Rep. 2017;7(1):41863. doi:10.1038/srep41863

[20] Sakamaki T, Ohtani E, Fukui H, et al. Constraints on earth's inner core composition inferred from measurements of the sound velocity of hcp-iron in extreme conditions. Sci Adv. 2016;2(2):e1500802. doi:10.1126/sciadv.1500802

[21] Hirao N, Kawaguchi IS, Hirose K, et al. New developments in high-pressure X-ray diffraction beamline for diamond anvil cell at SPring-8. Matter Radiat Extrem. 2020;5(1):018403. doi:10.1063/1.5126038

[22] Boccato S, Gauthier M, Siersch NC, et al. Picosecond acoustics: a new way to access elastic properties of materials at pressure and temperature conditions of planetary interiors. Phys Chem Minerals. 2022;49(6):20. doi:10.1007/s00269-022-01194-6
[23] Edmund E, Antonangeli D, Decremps F, et al. Structure and elasticity of cubic Fe-Si alloys at high pressures. Phys Rev B. 2019;100(13):134105. doi:10.1103/PhysRevB.100.134105
[24] Ohta K, Wakamatsu T, Kodama M, et al. Laboratory-based x-ray computed tomography for 3D imaging of samples in a diamond anvil cell in situ at high pressures. Rev Sci Instrum. 2020;91(9):093703. doi:10.1063/5.0014486
[25] Maslen EN. X-ray absorption. urn:lsbn:978-1-4020-1900-5. 2006;C:599–608.
[26] Dorogokupets PI, Dewaele A. Equations of state of MgO, Au, Pt, NaCl-B1, and NaCl-B2: internally consistent high-temperature pressure scales. High Press Res. 2007;27(4):431–446. doi:10.1080/08957950701659700
[27] Saito T, Matsuda O, Wright OB. Picosecond acoustic phonon pulse generation in nickel and chromium. Phys Rev B. 2003;67(20):205421. doi:10.1103/PhysRevB.67.205421
[28] Ohtani E, Shibazaki Y, Sakai T, et al. Sound velocity of hexagonal close-packed iron up to core pressures. Geophys Res Lett. 2013;40(19):5089–5094. doi:10.1002/grl.50992
[29] Antonangeli D, Morard G, Schmerr NC, et al. Toward a mineral physics reference model for the Moon's core. Proc Natl Acad Sci USA. 2015;112(13):3916–3919. doi:10.1073/pnas.1417490112
[30] Shibazaki Y, Nishida K, Higo Y, et al. Compressional and shear wave velocities for polycrystalline bcc-Fe up to 6.3 GPa and 800 K. Am Mineral. 2016;101(5):1150–1160. doi:10.2138/am-2016-5545
[31] Antonangeli D, Komabayashi T, Occelli F, et al. Simultaneous sound velocity and density measurements of hcp iron up to 93 GPa and 1100K: An experimental test of the Birch's law at high temperature. Earth Planet Sci Lett. 2012;331–332:210–214. doi:10.1016/j.epsl.2012.03.024
[32] Ohtani E, Shibazaki Y, Sakai T, et al. Sound velocity of hexagonal close-packed iron up to core pressures. Geophys Res Lett. 2013;40(19):5089–5094. doi:10.1002/grl.50992
[33] Mao Z, Lin J-F, Liu J, et al. Sound velocities of Fe and Fe-Si alloy in the Earth's core. Proc Natl Acad Sci USA. 2012;109(26):10239–10244. doi:10.1073/pnas.1207086109
[34] Wang S, Chen S, Qi X, et al. Reassessment of Birch's law on hcp-Fe from ultrasonic sound velocity measurement and implications on the velocity profiles of Earth's inner core. J Geophys Res: Solid Earth. 2024;129(5):e2023JB027979. doi:10.1029/2023JB027979
[35] Ikuta D, Ohtani E, Fukui H, et al. Sound velocity of hexagonal close-packed iron to the Earth's inner core pressure. Nat Commun. 2022;13(1):7211. doi:10.1038/s41467-022-34789-2
[36] Decremps F, Antonangeli D, Gauthier M, et al. Sound velocity of iron up to 152 GPa by picosecond acoustics in diamond anvil cell. Geophys Res Lett. 2014;41(5):1459–1464. doi:10.1002/2013GL058859